Rotational alignment in the photodesorption of CO from $Cr_2O_3(0001)$: A systematic three-dimensional *ab initio* study

S. Thiel, M. Pykavy, T. Klüner,[a] and H.-J. Freund
Fritz-Haber-Institut der Max-Planck-Gesellschaft, Faradayweg 4-6, 14195 Berlin, Germany

R. Kosloff
Department of Physical Chemistry and the Fritz Haber Research Center, The Hebrew University of Jerusalem, Jerusalem 91404, Israel

V. Staemmler
Ruhr-Universität Bochum, Lehrstuhl für Theoretische Chemie, Universitätsstrasse 150, 44780 Bochum, Germany

(Received 25 July 2001; accepted 15 October 2001)

In recent experiments, the rotational alignment of the laser induced nonthermal desorption of CO adsorbed on an epitaxially grown film of $Cr_2O_3(0001)$ has been studied [Beauport, Al-Shamery, and Freund, Chem. Phys. Lett. **256**, 641 (1996)]. At low-rotational quantum numbers J, the molecules desorb like helicopters (J-vector perpendicular to the surface) while at high J-values cartwheel motion is preferred (J-vector parallel to the surface). These stereodynamic effects and the experimental state resolved velocity distributions of the desorbing species are simulated by means of an exact time-dependent wave packet method in three dimensions. As a basis for this quantum-mechanical treatment of the CO desorption *ab initio* potential energy surfaces (PES) were used. The PES for the electronic ground state of the $CO–Cr_2O_3(0001)$ system has been calculated previously by Pykavy *et al.* [Surf. Sci. **479**, 11 (2001)] in an embedded cluster approach. As the intermediate state, generated by the laser irradiation, an internal CO excited state ($5\sigma \rightarrow 2\pi^*$) was considered. The PES of this $a\ ^3\Pi$-like state of CO adsorbed on $Cr_2O_3(0001)$ was calculated at the *ab initio* CASSCF-level. Our key findings in the subsequent wave packet calculations are (1) a high-dimensional treatment of the photodesorption process is very important in this system, essentially the angular coordinates, very often neglected in similar studies, are responsible for a ''successful'' desorption event; (2) the change from the strongly tilted equilibrium geometry in the electronic ground state to the preferred upright position in the electronically excited state after laser irradiation is essential for the mechanistic picture of the desorption process; (3) the experimental phenomemon of rotational alignment can only be explained if the topologies of the PES of both the electronically excited and the ground state are accounted for; (4) the lifetime of the CO*-intermediate is in the order of 10 fs; (5) the molecule–surface vibrations in the electronic ground state do not much influence the asymptotic results at the experimental temperature of $T = 100$ K. However, the inclusion of excited levels of the hindered rotation helps to gain insight into the desorption mechanism on a microscopic level. © *2002 American Institute of Physics.*
[DOI: 10.1063/1.1425383]

I. INTRODUCTION

In addition to adsorption, diffusion, and reaction, the desorption of molecules is an essential step in chemical reactions at surfaces. Desorption can be caused either by heating the surface or by irradiation with laserlight of a fixed wavelength. While thermal energy in principle excites all degrees of freedom of the system, laser irradiation exclusively populates certain states. This difference implies the use of quantum mechanical methods to model a photodesorption event. The recent example of CO oxidation on the ruthenium(0001)-surface might serve to illustrate those principles.[1] Heating the ruthenium(0001) surface with CO and oxygen coadsorbed results in the desorption of CO. Laser irradiation of this system with infrared femtosecond laser pulses, on the other hand, allows for CO oxidation, followed by CO_2 desorption. This example emphazises the relevance of charge and energy transfer for the microscopic understanding of a photodesorption event.[2]

The well known theoretical models used to describe photodesorption of small molecules from surfaces are based on the geometrical configurations of two electronic states, of the electronic ground state and an electronically excited state of the adsorbate–substrate system. The change in distance of the adsorbed molecule from the surface after laser excitation is often considered to be the driving force which enables desorption when the system relaxes to its electronic ground state. In the interpretation of Menzel, Gomer, and Redhead[3,4] the molecule feels a repulsive potential after laser excitation, which accelerates the molecule towards larger distances from

[a]Author to whom correspondence should be addressed. Electronic mail: kluener@fhi-berlin.mpg.de

the surface as compared to the electronic ground-state equilibrium distance. Depending on the lifetime of this electronically excited state the molecule can gain sufficient kinetic energy to desorb after relaxation to the electronic ground state. In the Antoniewicz picture the molecule is accelerated towards smaller distances after laser excitation and is scattered at the surface after relaxation.[5] In this case the lifetime of the electronically excited state limits the success of the photodesorption event as well. Reasonable values for this lifetime are in the order of femtoseconds.

These two models are generally treated as one-dimensional models, taking into account the center-of-mass distance of the molecule from the surface as the desorption coordinate. It is challenging though to gain more detailed mechanistic insight into the photodesorption process by considering more than one degree of freedom of the adsorbed molecule. In some theoretical investigations of photodesorption from surfaces two dimensions were included,[6] the second degree of freedom very often being the internal molecular vibration.[7–11] A two-dimensional picture was necessary, for example, to understand isotope effects in the photon- or electron stimulated desorption of the ammonium-molecule from surfaces.[12–15]

To obtain a complete picture of the photodesorption process, it is necessary to improve the theoretical methods which are used to describe this process. In this context stochastic wave packet methods and direct methods to solve the Liouville von Neumann equation for open systems were compared.[16] In those studies the system NO–Pt(111) was investigated extensively.[6] To develop a complete microscopic model of a photodesorption process from surfaces it is important to address the decay of the electronically excited state which is populated by the laser irradiation. In this context the idea of a ''surrogate'' Hamiltonian to describe the dissipative dynamics of an adsorbate on a surface turns out to be promising.[17,18] Methods involving the system–environment interaction with external laser fields present are currently under development.[19] Different propagation methods were compared in a recent study investigating the effect of substrate vibrations on the sticking of hydrogen-atoms at surfaces.[20]

Apart from the question of dimensionality and the theoretical treatment, the topology of the potential energy surfaces plays an important role. It is necessary to rely on potential energy surfaces which are not based on empirical assumptions but on first principles, especially for the electronically excited states. The first example for a successful description of a photodesorption event in a complete *ab initio* picture was the desorption of NO-molecules from the NiO(100) surface.[21] Experimental observables such as desorption yield and the velocity distribution of the desorbed molecules were reproduced on the basis of a two-dimensional *ab initio* potential energy surface for a representative excited charge transfer state. The second degree of freedom taken into account was the polar angle of the adsorbate with respect to the surface normal. To describe the scalar experimental observables of the NO–NiO-system a two-dimensional model turned out to be sufficient. Quantitative agreement between experimental and theoretical vibrational state populations was obtained for this system as well. For this purpose it had been necessary to include the internal distance of the NO^- intermediate, which was done by means of Hartree–Fock calculations.[22]

As an example for a high-dimensional time independent quantum dynamical treatment of an adsorbate–substrate system we would like to mention the adsorption and desorption of H_2 on the palladium(100) surface.[23] The sticking coefficient of the hydrogen-molecule as a function of the initial kinetic energy, which had been measured in scattering experiments, could be simulated by performing time-independent scattering calculations on a six-dimensional electronic ground-state potential energy surface of the H_2–Pd(100)-system. Due to the small number of rotational states populated, a high-dimensional quantum dynamical treatment of the H_2-molecule is feasible. The situation of the CO-molecule is very much different because its large moment of inertia causes the rotational levels spacings to narrow. Therefore, a quantum dynamical treatment of the CO motion becomes already very demanding for lower dimensionality as compared to the H_2 motion.

To gain mechanistic insight into vectorial effects such as rotational alignment, observed, e.g., in the CO–Cr_2O_3-system,[24] high dimensionality in combination with the use of *ab initio* potential energy surfaces for both the electronic ground *and* electronically excited state is compulsory. In a short letter, we presented a microscopic picture for the desorption process of the CO–Cr_2O_3-system[25] which was gained by performing the first three-dimensional *ab initio* quantum dynamical study of photodesorption from solid surfaces. In this study we present a detailed systematic three-dimensional treatment of the photodesorption of CO from the Cr_2O_3(0001)-surface. A stochastic wave packet approach is used on the basis of *ab initio* potential-energy surfaces for the electronic ground state and a representative electronically excited state populated by the laser irradiation. The stochastic approach causes huge computational effort, since a large number of single three-dimensional (3D) quantum trajectories has to be followed and incoherently averaged.[16]

After this introduction, Sec. II will shortly review the experimental results for this system. In Sec. III, we qualitatively describe the construction and the topology of two representative potential energy surfaces involved in the desorption process. Section IV then deals with the subsequent wave packet dynamics on these PES, followed by the essential conclusions in Sec. V.

II. EXPERIMENT

The geometric structure of the polar Cr_2O_3(0001)-surface is fairly well known from LEED-experiments and *ab initio* calculations.[26,27] It was found in those studies that the surface is chromium terminated, but in the terminating chromium layer only half of the available cation positions are occupied. This structure of the Cr_2O_3(0001)-surface is the basis for the construction of the electronic potential energy surfaces discussed in Sec. III. CO-molecules chemisorb weakly on this half terminated Cr_2O_3(0001)-surface. Thermal desorption occurs at 160 K corresponding to an adsorption energy of 43 kJ/mol.[28]

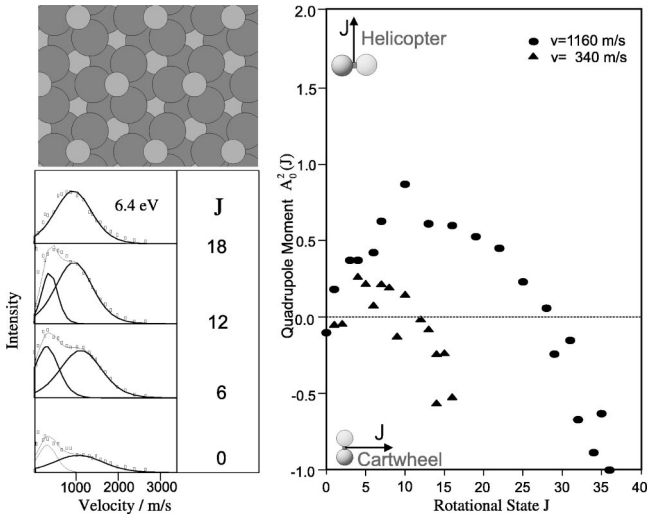

FIG. 1. Experimental results after photodesorption of CO from the $Cr_2O_3(0001)$-surface with 6.4 eV radiation. *Left*: Geometrical structure of the terminating layer (top), velocity distributions as function of the desorbate rotational state (bottom)—*Right*: quadrupole moment of desorbing CO as function of rotational state for a low and a high velocity.

In the photodesorption experiments,[24] the CO-molecules were desorbed by 6.4 eV laser pulses of the wavelength 193 nm and a duration of about 15 ns. After a well defined time delay between desorption and detection the desorbed molecules were detected quantum state resolved via a REMPI $[1+1]$ (resonance enhanced multiphoton ionization) scheme.[29] Figure 1 shows velocity distributions of the desorbing species in its vibrational ground state on the left. For some rotational quanta bimodal features as in the extensively studied NO–NiO-system[30–32] are observed. In the present study we focus only on the velocity of the desorbing molecule. This ranges from 0 to 2000 m/s.

By changing the polarization of the detection laser, rotational alignment effects of the desorbing CO-molecules, i.e., the direction of the total angular momentum vector J, could be observed. In the system $CO–Cr_2O_3(0001)$ it was found that CO-molecules desorbing with low rotational excitation (rotationally cold molecules) desorb like a helicopter with the total angular momentum vector oriented parallel to the surface normal. CO-molecules with high rotational excitation (rotationally hot molecules) desorb like a cartwheel with the total angular momentum vector oriented perpendicular to the surface normal. These effects are shown in Fig. 1 (right). From the REMPI-intensities of parallel and perpendicular polarized light the quadrupole moment $A_0^{(2)}(J)$ of the desorbing CO-molecule can be deduced.[33] The value $A_0^{(2)}=2$ corresponds to a perfect helicopter molecule, $A_0^{(2)}=-1$ to a perfect cartwheel. For two desorption velocities this quadrupole moment $A_0^{(2)}$ is shown in Fig. 1. As mentioned before, the direction of the total angular momentum vector changes as a function of the rotational quantum number. This corresponds to a change from helicopter motion to cartwheel motion with increasing rotational excitation. This stereodynamic effect enlarges the knowledge of scalar observables known from former photodesorption experiments in oxide systems.[30–32]

III. POTENTIAL ENERGY SURFACES

A. Electronic ground-state PES

In order to understand and analyze the experimental results presented in the previous section, quantum-mechanical simulations of the desorption process were performed on a complete *ab initio* basis. At a first stage, potential energy surfaces (PES) both for the electronic ground state and the electronically excited state involved were calculated in the framework of the Born–Oppenheimer approximation. Since the adsorption of CO on the $Cr_2O_3(0001)$-surface is a local process, quantum chemical cluster calculations were employed for the determination of the PES.[28] The $Cr_2O_3(0001)$-surface was represented by a finite neutral Cr_4O_6-cluster embedded in an extended point charge field. The motion of the CO-molecule above the $Cr_2O_3(0001)$-surface was investigated with respect to four coordinates: The center-of-mass distance Z from the surface as the ''desorption coordinate,'' the polar angle θ $(0°\leqslant\theta\leqslant180°)$ of the C–O axis with respect to the surface normal, the azimuthal angle ϕ $(0°\leqslant\phi\leqslant360°)$ and the one-dimensional lateral translation coordinate X, describing the motion of the CO center-of-mass along the Cr–Cr-axis. The two angular coordinates θ and ϕ are essential to address the stereodynamical effect described in Sec. II.

The lateral translation X is frozen at its ground-state equilibrium value in the subsequent wave packet calculations. This corresponds to a position of the CO-molecule where the center-of-mass is located in the middle of the Cr–Cr-axis. The geometry of the substrate, both of the Cr_4O_6-cluster and of the embedding point charge field, was fixed at the optimum structure of the $Cr_2O_3(0001)$-surface;[28] the C–O bond length was fixed at its equilibrium gas-phase value of 2.13 a.u. The total energy calculations were performed using the Bochum open shell *ab initio* package.[34–37] For the PES of the ground state, the calculations were performed within the restricted open shell Hartree–Fock approximation with basis sets of triple zeta quality. The basis set superposition error (BSSE) was taken into account applying the counterpoise correction by Boys and Bernardi.[38] Details of the electronic structure calculations can be found elsewhere.[28] In Fig. 2 we show a two-dimensional θ-ϕ contour plot of the PES of the electronic ground state at the equilibrium value of the center-of-mass distance coordinate Z. The ground-state PES exhibits its absolute minimum at an azimuthal angle of $\phi=180°$ which corresponds to an inline configuration of the CO-molecule with respect to the Cr–Cr-axis, as shown in the inset of Fig. 2. The minimum with respect to the polar angle is located at $\theta=120°$. This means that the CO-molecule is very strongly tilted in the electronic ground state of the adsorbate–substrate system ($\theta=0°$ is the upright O-end down geometry, $\theta=90°$ corresponds to a flat geometry). If the CO-molecule is rotated by 180° with respect to ϕ, a local minimum is reached after crossing an energy barrier of 40 kJ/mol. This local minimum at $\phi=0°$ (and at $\phi=360°$ due to the periodicity of ϕ) exhibits a smaller binding energy (only 15 kJ/mol) but corresponds to a stronger tilted adsorption geometry of $\theta=110°$. Occupation of this local minimum would end in a nearly flat adsorption

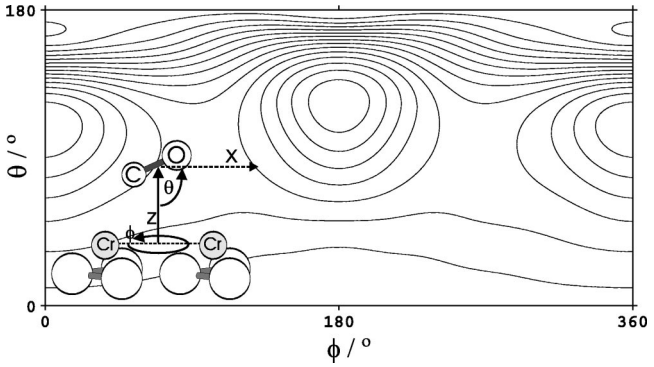

FIG. 2. 2D contour plot of the electronic ground-state *ab initio* PES for the CO–Cr_2O_3(0001) system: $\theta-\phi$-dependence at the equilibrium value for CO center-of-mass distance ($Z=4.5$ Bohr). The lateral translation coordinate X is frozen at the equilibrium value, which corresponds to a position of the CO-molecule in the middle of the Cr–Cr-axis. The two Cr-ions of the second layer included in the Cr_4O_6-cluster are not shown.

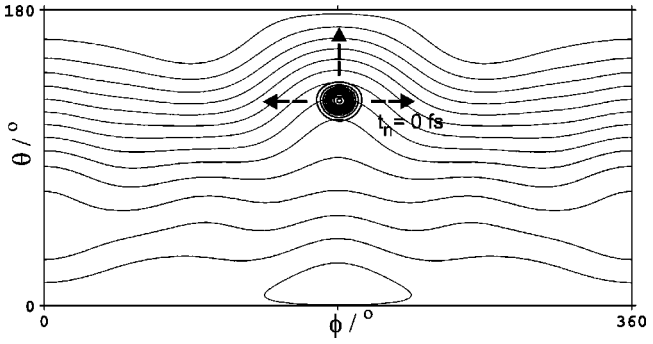

FIG. 3. 2D contour plot of the electronically excited $a\,^3\Pi$-like state *ab initio* PES for the CO–Cr_2O_3(0001) system: $\theta-\phi$-dependence at the electronic ground-state equilibrium value for the CO center-of-mass distance ($Z=4.5$ Bohr). This corresponds to the Franck–Condon point for Z. The rovibrational ground-state wave packet is positioned onto this PES, modeling a sudden vertical transition caused by the laser irradiation.

geometry. In NEXAFS-experiments evidence was found for a very strongly tilted adsorbed CO-species.[39] This electronic ground-state potential energy surface underestimates the experimental CO binding energy of 43 kJ/mol by about 16 kJ/mol.[28] Even the inclusion of dynamic correlation effects by MCCEPA (multiconfiguration coupled electron pair approximation)—calculations does not account for this difference. A detailed comparison between theoretical electronic ground-state calculations and experimental findings for the CO–Cr_2O_3-system was performed recently.[28] It should be noted that general features of the topology of the two dimensional (2D) contour shown in Fig. 2 do not change if the center-of-mass distance Z is varied. This implies that the consideration of the electronic ground-state PES is not sufficient to account for the stereodynamic effects found in experiment.

B. Excited-state PES

To simulate a photodesorption process on an *ab initio* basis, the knowledge of electronically excited states populated by the laser irradiation is essential. The state most likely involved as desorption intermediate results from an internal CO $5\sigma\rightarrow 2\pi^*$ excitation. An internally excited CO-molecule as intermediate is in contrast to the popular model of a negative ion resonance, which is mostly employed in the discussion of the photodesorption of small diatomic molecules (mainly NO) from metal and insulator surfaces.[40] However, contrary to NO^-, CO^- is not a stable molecule in the gas phase. It could be possible that the negative ion resonance is stabilized in the electrostatic field above the Cr_2O_3(0001)-surface. Therefore, CO^- cannot be ruled out as an intermediate. On the other hand, there is no experimental information about the nature of the excited state. The energetically lowest $5\sigma\rightarrow 2\pi^*$-state is the $a\,^3\Pi$-like state with an excitation energy very close to the experimental laser energy of 6.4 eV. We have selected the $a\,^3\Pi$-like state of CO as a representative electronically excited state, although the transition into it is optically forbidden. This can be justified, since it is not clear if the excitation can be described as an optical transition or as being mediated via electron hole pairs. The $2\pi^*$ orbital, which determines the topology of the excited state PES to a large extent, is singly occupied. Therefore, the angular topologies of the PES of the $a\,^3\Pi$-like state and the $a\,^1\Pi$-like state and also of the lowest CO^- resonance are very similar. A four-dimensional (4D) PES for the $a\,^3\Pi$-like state was calculated by the complete active space SCF (CASSCF) method. The active space includes the 5σ and $2\pi^*$ orbitals involved in the CO-excitation and in addition the $3d$-orbitals of the two top Cr-ions in the Cr_4O_6-cluster. Details of the calculation can be found elsewhere.[41] As for the ground state PES, the lateral translation coordinate X was frozen at the equilibrium value. Figure 3 shows the $\theta-\phi$ dependence of the PES for the electronically excited $a\,^3\Pi$-like state at the ground-state equilibrium value of the desorption coordinate Z. This is the $\theta-\phi$ potential which the nuclear rovibrational ground-state wave packet experiences if it is placed by a sudden vertical transition due to the laser irradiation to the excited state. The excited-state PES has a large gradient with respect to θ which forces the CO-molecule to move from the strongly tilted ground-state equilibrium geometry towards an upright adsorption geometry. At the same time, the excited CO-molecule is accelerated with respect to the azimuthal angle ϕ, hence the CO-molecule starts to rotate within the plane parallel to the surface. In Fig. 4 we quantify those effects. The corrugation with respect to the azimuthal angle ϕ in the excited state is inverted as compared to the electronic ground state. This can be seen in the one-dimensional cuts of the two PES at the equilibrium values for θ, Z, and X (Fig. 4, left). The two topologies have their origin in the electrostatic interaction between the quadrupole moment of the CO molecule and the field gradients at the surface. The instantaneous excitation indicated by the upward arrow transfers the nuclear ground-state wave packet to a region where it experiences an average ϕ-gradient in the Franck–Condon region of 1.5×10^{-4} Hartree per degree. The absolute ϕ-corrugation within the excited state (0.010 a.u.) is smaller than in the electronic ground state (0.015 a.u.). With respect to the polar angle θ, on the other hand, the nuclear wave packet experiences a

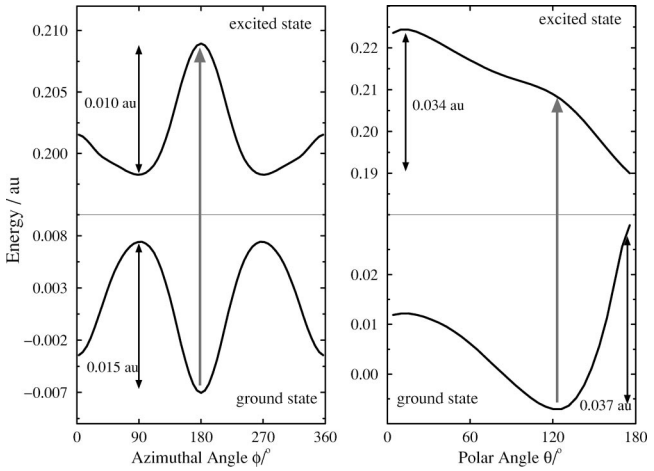

FIG. 4. 1D cuts through electronic ground- and excited-state PES. *Left*: ϕ-corrugation at $\theta=120°$ and $Z=4.5$ a.u. *Right*: θ-dependence at $\phi=180°$ and $Z=4.5$ a.u. The upward arrow indicates a vertical sudden transition.

significantly larger gradient of 3.4×10^{-4} Hartree per degree after sudden transition to the excited-state PES at the Franck–Condon point.

The two representative *ab initio* PES discussed in this section are the basis for quantum-dynamical studies of the photodesorption process within a two-state model. However, before the two PES, which have been calculated pointwise, can be used in the quantum-mechanical wave packet calculation, they must be cast into an analytical form. In the present study, we fix the translation along X to its equilibrium value of the electronic ground state and consider only the degrees of freedom Z, θ, and ϕ. The functional form is given by

$$V_{g,e}(Z,\theta,\phi)=u_0+u_1/Z^3+u_2/Z^4 + u_3\exp(-u_4(Z-u_5)^2), \tag{1}$$

for both PES ($g=$ ground state, $e=$ excited state), where u_i ($i\neq0$) are Fourier expansions in the angular coordinates θ and ϕ

$$u_i=\sum_{j=0}^{N} v_{ji}\cos(j\phi) \quad \text{for } i=1,\ldots,5,$$

$$v_{ji}=\sum_{k=0}^{N-1} a_{kji}\cos(k\theta)+\sum_{k=1}^{N-1} b_{kji}\sin(k\theta) \quad \text{for } j=0,$$

$$v_{ji}=\sum_{k=1}^{N-1} c_{kji}\sin(k\theta) \quad \text{for } j\neq0.$$

The fit parameters u_0, a_{kji}, b_{kji}, and c_{kji} were determined by means of a least-squares method. (electronic ground state: $N=4$; electronically excited state:[41] $N=3$). The fit parameters are provided to the interested reader on request.

IV. DYNAMICS

A. Propagation method

A purely quantum-mechanical wave packet method based on the time-dependent Schrödinger equation

TABLE I. Numerical parameters used in the 3D quantum wave packet calculations. All parameters are given in atomic units.

Constants		
Mass CO-molecule	M	51 040.8724 a.u.
Moment of inertia CO-molecule	I	56 829.7084 a.u.
Reduced mass CO-molecule	μ	12 499.8055 a.u.
Internal C–O-distance	τ_e	2.13 a.u.
Z-Grid		
Start	$Z_{\min}$	2.0 a.u.
End	$Z_{\max}$	15.0 a.u.
Grid points	N_Z	256
Grid spacing	ΔZ	0.051 a.u.
Maximum momentum	$k_{z\max}$	61.6 a.u.
Momentum resolution	ΔkZ	0.48 a.u.
Grid change		
Center of transfer function	Z_0	12.5 a.u.
Width of transfer function	a	6.0 a.u.
Asymptotic grid start	$Z2_{\min}$	10.16 a.u.
Asymptotic grid end	$Z2_{\max}$	16.63 a.u.
Asymptotic grid points	$N2_Z$	128
Asymptotic grid spacing	ΔZ_2	0.051 a.u.
Maximum asymptotic momentum	$k2_{z\max}$	61.6 a.u.
Asymptotic momentum resolution	ΔkZ_2	0.96 a.u.
θ-Grid		
Grid points	N_θ	83 (zeros of P_{83}^0)
Maximum rotational state	$J_{\max}$	82
ϕ-Grid (periodic in $[0:2\pi]$)		
Start	$\phi_{\min}$	0.02 a.u.
End	$\phi_{\max}$	6.26 a.u.
Grid points	N_ϕ	165
Grid spacing	Δ_ϕ	0.04 a.u.
Maximum projection quantum number	$M_{\max}$	82
M-space resolution	ΔM	1
Propagation		
Time Step (excited state)	Δt	10 a.u.
Spacing of excited state lifetime grid	Δt_n	50 a.u.
Number of quantum trajectories	$n_{\max}$	80
Time step (ground state)	Δt	50 a.u.
Total propagation time	t	60 000 a.u.

$$i\frac{\partial\Psi_{g,e}(Z,\theta,\phi,t)}{\partial t}=\hat{H}_{g,e}(Z,\theta,\phi)\Psi_{g,e}(Z,\theta,\phi,t), \tag{2}$$

for the nuclear wave function $\Psi_{g,e}(Z,\theta,\phi,t)$ is employed. Within the 3D model the Hamiltonian contains the potential energy $V_{g,e}(Z,\theta,\phi)$ of Eq. (1) and kinetic-energy terms in the center-of-mass coordinate Z and the two angular coordinates θ and ϕ

$$\hat{H}_{g,e}(Z,\theta,\phi)=-\frac{1}{2\mu r_e^2}\left(\frac{1}{\sin\theta}\frac{\partial}{\partial\theta}\sin\theta\frac{\partial}{\partial\theta}+\frac{1}{\sin^2\theta}\frac{\partial^2}{\partial\phi^2}\right) - \frac{1}{2M}\frac{\partial^2}{\partial Z^2}+\hat{V}_{g,e}(Z,\theta,\phi), \tag{3}$$

where $\hat{V}_{g,e}(Z,\theta,\phi)$ are the *ab initio* potential energy surfaces for the electronic ground state (g) and the electronically excited state (e) presented in Sec. III. M and μ are the total mass and the reduced mass of the CO-molecule, respectively, with the internal C–O-distance held fixed at its equilibrium value $r_e=2.13$ a.u.

For the coordinate Z an equidistant grid is set up and fast Fourier transform (FFT) techniques are used to calculate the

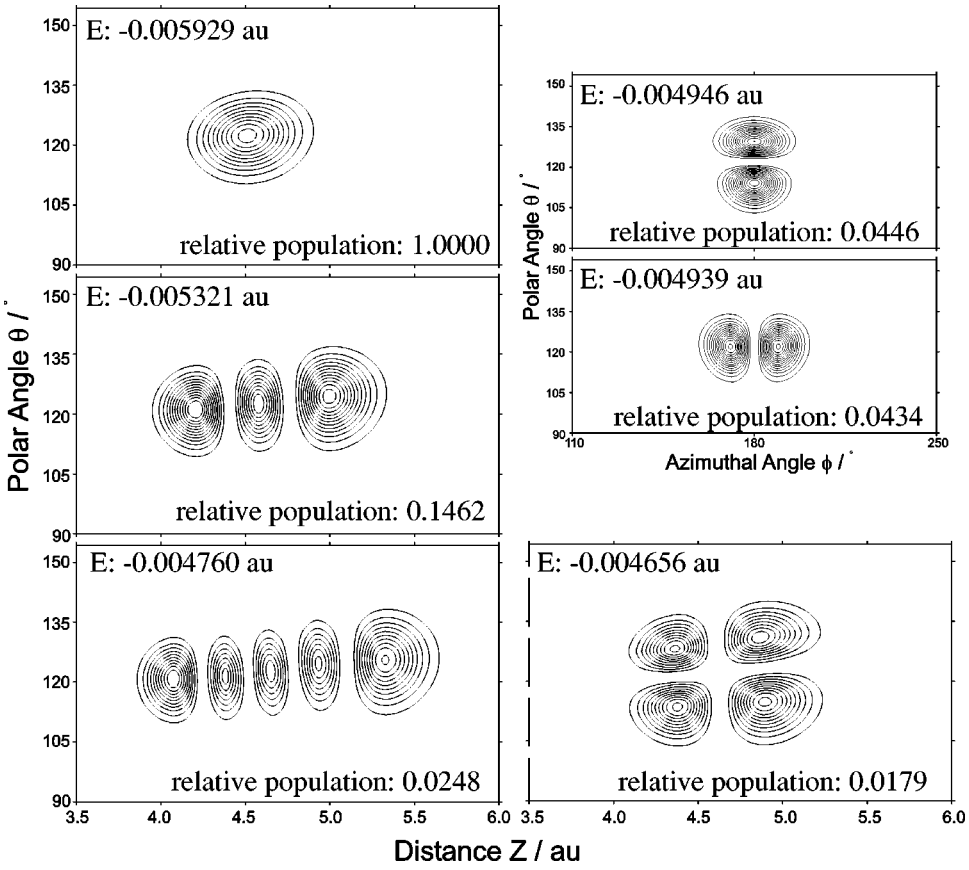

FIG. 5. Eigenstates of the three-dimensional electronic ground-state PES. *Left*: Excitation of molecule–surface vibration. *Right*: Excitation of frustrated rotation. Absolute energies E and relative populations P/P_0 at the experimental temperature of $T=100$ K are given. The $Z-\theta$ distributions are shown for the azimuthal equilibrium configuration ($\phi=180°$). The $\theta-\phi$ distributions are shown for the equilibrium center-of-mass distance ($Z=4.5$ a.u.).

translational kinetic-energy operation $\hat{T}_{\text{trans}}\Psi$ in momentum space.[42] The grid change technique proposed by Heather and Metiu[43] is applied for this coordinate to separate and analyze the desorbing part of the wave packet and to prevent reflection of the wave packet at the grid boundary at large Z. Those parts of the wave packet which travel towards the asymptotic region of the electronic ground-state potential (beyond Z_0) are considered as desorbed. Accordingly, in each time step the wave packet is multiplied by a smooth ''transfer function''

$$f_{\text{trans}}=\frac{1}{(1+\exp(a\cdot(Z-Z_0)))}. \tag{4}$$

The rotational part $\hat{T}_{\text{rot}}$ of the kinetic-energy operator is used within the Gauss–Legendre scheme proposed by Corey and Lemoine.[44] This scheme needs an equidistant grid with periodic boundaries for the azimuthal coordinate ϕ in the interval $[0{:}2\pi]$ to account for a full rotation of the CO-molecule in a plane parallel to the surface. The grid for the polar angle θ is defined in the interval $[0{:}\pi]$, the grid points are located at the zeros of the Legendre polynomial $P^0_{N_\theta}(\cos\theta)$, where N_θ is the number of grid points. The maximum rotational quantum number which can be represented on this angular momentum grid is $j_{\max}=N_\theta-1$. After the Gauss–Legendre transform the rotational energy operation consists of a simple multiplication with the rotational energy eigenvalue spectrum $l(l+1)/2\mu r_e^2$.

To calculate the time evolution, we use the Feit–Fleck split propagator.[45] The numerical results for the observables of interest have been carefully checked and compared versus the Chebychev propagator[46] which serves as a very accurate reference. The parameters for propagation and grids are given in Table I.

The photodesorption process is described as a DIET (desorption induced by electronic transitions)—process in a two-state model. The two states involved are the electronic ground state (g) and the electronically excited state (e) considered in the previous section. We treat the DIET-process using Gadzuk's jumping wave packet method[47,48]

$$\Psi(t;t_n)=e^{-i\hat{H}_g(t-t_n)}e^{-i\hat{H}_e t_n}\Psi(0). \tag{5}$$

The rovibrational nuclear wave function $\Psi(0)$ of the electronic ground state is transferred in a first step vertically up to the electronically excited state and evolves in this state up to the residence time t_n. The wave function is then transferred vertically down to the electronic ground state, where it evolves to a final time t. At this time t, the observables of interest are converged with respect to propagation time. Expectation values of operators $\hat{A}$ as a function of this single-trajectory residence time t_n are then calculated as

$$A(t;t_n)=\langle\Psi_{\text{des}}(t,t_n)|\hat{A}|\Psi_{\text{des}}(t,t_n)\rangle, \tag{6}$$

and averaged incoherently with respect to a coordinate independent resonance lifetime τ of the exponentially decaying electronically excited state

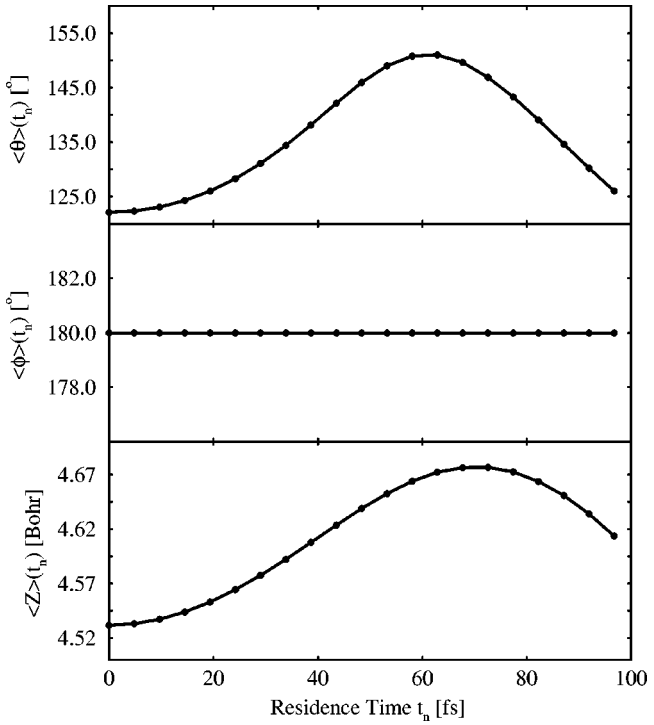

FIG. 6. Expectation values $\langle\theta\rangle$ (upper panel), $\langle\phi\rangle$ (middle panel), and $\langle Z\rangle$ (lower panel) of the rovibrational ground-state wave packet evolving on the electronically excited $a\,^3\Pi$-like state PES.

$$A(t;\tau)=\frac{\sum_{n=1}^{n_{\max}} A(t;t_n)\exp\left(-\frac{t_n}{\tau}\right)}{\sum_{n=1}^{n_{\max}} \exp\left(-\frac{t_n}{\tau}\right)}. \tag{7}$$

Ψ_{des} denotes the ''desorbed'' part of the wave packet, which is located in the asymptotic region of space at time t. The computer times necessary for the 3D wave packet calculations in this jumping wave packet picture are rather large, since high kinetic and rotational energies occur for the heavy CO-molecule. Due to the large moment of inertia of the CO-molecule, many rotational states are populated during the propagation. The correct description requires more than 3×10^6 grid points in the 3D Z, θ, ϕ space. A single nonaveraged quantum trajectory took about one day of CPU-time on a workstation (SGI R10000) for a total propagation time t of about 1.5 ps. The number of quantum trajectories [$n_{\max}$ in Eq. (7)] which is necessary to get a converged result in the lifetime averaging procedure is in the order of 100.

B. Electronic ground-state eigenfunctions

By propagation in imaginary time,[49] the lowest stationary nuclear eigenfunctions of the electronic ground-state PES were calculated. The lowest energy levels correspond to excitation of the molecule–surface vibrational mode. Some of them are shown in Fig. 5. Excitation of the molecule-surface bond becomes visible by the increasing number of nodes along the Z coordinate as shown on the left part of Fig. 5. The energies and relative populations, assuming a Boltzmann distribution for the experimental temperature of $T=100\,\mathrm{K}$ are given in Fig. 5. Only the first three molecule–surface vibrational levels are significantly populated. In contrast to the situation in gas phase, rotational excitation occurs only at relatively high energies. This is due to the corrugation of the electronic ground-state PES with respect to the angular coordinates θ and ϕ. The two nearly degenerate levels with nodes in θ and ϕ in the top right part of Fig. 5 correspond to hindered rotations. Although they are not significantly populated at the experimental temperature, they help to gain insight into the microscopic desorption mechanism discussed within the next paragraphs. Furthermore, they take part in the discussion of laser control in the sense of preexcitation of separate adsorbate–substrate energy levels.[50]

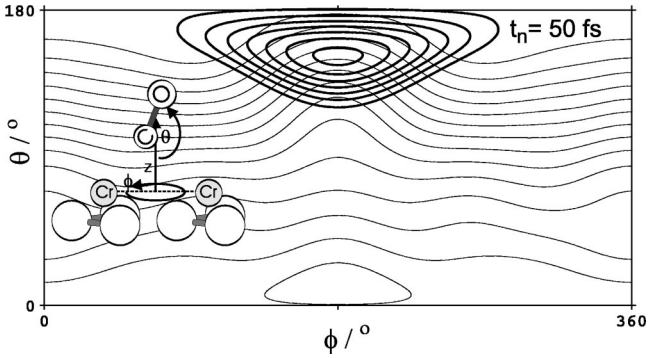

FIG. 7. $\theta-\phi$-snapshot of rovibrational ground-state wave packet after time evolution of 50 fs on the PES of the electronically excited state. The CO molecule has left its strongly tilted equilibrium geometry towards an upright adsorption geometry. Simultaneously, the molecule starts to rotate within a plane parallel to the surface.

C. Excited-state dynamics

In the limiting case of $T=0\,\mathrm{K}$, only the rovibrational ground-state nuclear wave function of the electronic ground-state PES is populated. At $t=0$ it is transferred vertically to the electronically excited $a\,^3\Pi$-like state, where it will evolve in time. In Fig. 6 we show the expectation values $\langle\theta\rangle$, $\langle\phi\rangle$, and $\langle Z\rangle$ as a function of the residence time t_n in the excited state. The polar angle θ increases within the range 0–60 fs. This is the change from the strongly tilted adsorption geometry in the electronic ground state towards an upright geometry during the time evolution on the PES of the excited state. The θ behavior in a time interval of 100 fs is characterized by a ''hindered rotation'' of the adsorbed CO-molecule after being excited. This motion is accompanied by a spread of the wave packet with respect to ϕ, because of the weak azimuthal ϕ-gradient discussed in Sec. III. This means, the laser excites a hindered cartwheel rotation of the CO-molecule and simultanously a slight helicopter motion. This motion is visible in Fig. 7, containing a snapshot of the rovibrational ground-state wave packet after a time evolution of 50 fs on the electronically excited-state PES.

As both PES involved in this desorption process are symmetric in the azimuthal angle ϕ with respect to $\phi=180°$, the expectation value $\langle\phi\rangle$ remains constant during the simulation. For t_n up to 70 fs the wave packet moves towards larger separation Z from the surface, which is typical for an MGR-type scenario.[3,4] The topology of the electronically excited $a\,^3\Pi$-like state PES in the region of large

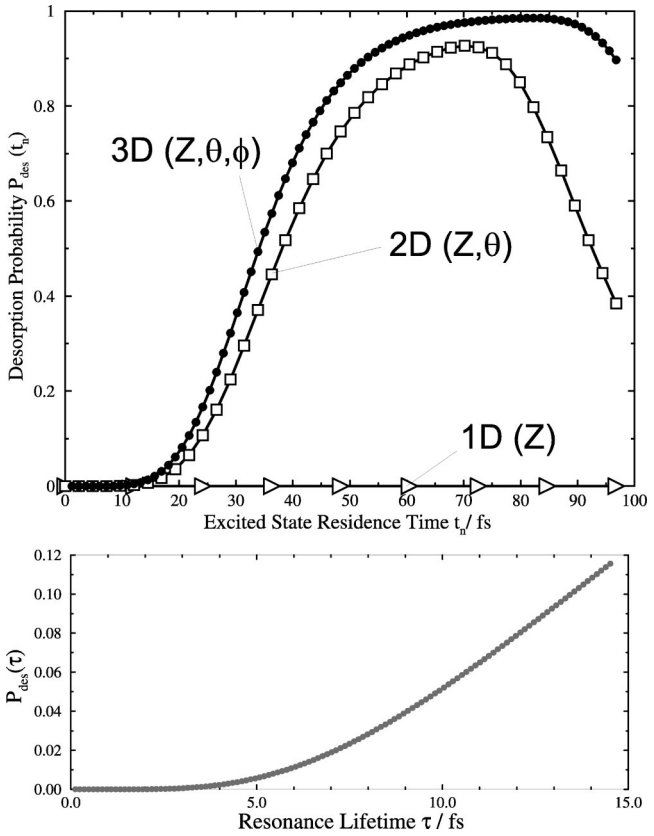

FIG. 8. *Top*: Asymptotic desorption probability $P_{\mathrm{des}}(t_n)$; open triangles: 1D-calculations in Z with θ and ϕ frozen at ground-state equilibrium values; open squares: 2D-calculation in Z and θ with ϕ frozen; filled circles: 3D-calculation in Z, θ, and ϕ. *Bottom*: Lifetime averaged desorption probability (from 3D calculations) as a function of the resonance lifetime τ.

values of θ forces the wave packet to move back towards the surface at later time. The amplitude of this oscillation in the Z coordinate is very small and amounts only to about 0.15 Bohr. This means that the laser excitation does not lead to a pronounced motion of the CO-molecule along the desorption coordinate in the electronically excited state. We will show later in this study that the angular coordinates are of more importance for the microscopic desorption mechanism. Therefore, it is not reasonable to distinguish between the two well-known one-dimensional MGR and Antoniewicz desorption mechanisms in this case.[3–5]

D. Desorption probability

After transition from the electronically excited state to the ground state the individual quantum trajectories are calculated up to a final time of 1.5 ps. The desorption probability per excitation event is calculated as the square norm of the desorbing part of the wave packet (Ψ_{des}), separated by the grid change technique as mentioned in Sec. IV

$$P_{\mathrm{des}}(t;t_n)=\langle \Psi_{\mathrm{des}}(t,t_n)|\Psi_{\mathrm{des}}(t,t_n)\rangle. \tag{8}$$

In Fig. 8 the question of dimensionality is addressed. One-dimensional calculations with respect to the coordinate Z were performed after ''freezing'' the angular coordinates θ and ϕ at their ground-state equilibrium values ($\theta=120°$ and $\phi=180°$). For the $CO–Cr_2O_3$ system the desorption probability is close to zero for all residence times t_n [e.g., $P_{\mathrm{des}}(50\,\mathrm{fs})=1.25\times10^{-10}$], thus a 1D-treatment is certainly not sufficient. If the polar angle is also taken into account, a drastic increase in the desorption probability is found, which strongly depends on the residence time t_n. This increase clearly proves the importance of the angular coordinates. The change in adsorption geometry in the excited state is crucial for the microscopic desorption mechanism. Desorption can only occur after the CO-molecule has left its strongly tilted ground-state equilibrium geometry and has moved towards an upright geometry. The electronic ground-state PES becomes repulsive with respect to Z if the polar angle is increased. The topology of the PES of the excited state enables this increase in θ. 3D calculations in Z, θ, and ϕ result in a further increase of $P_{\mathrm{des}}(t_n)$, but the difference is not as large as that from the 1D- to the 2D-picture. At this stage it is already clear that it is primarily the angular coordinates which are responsible for the success of the desorption event and not so much the dependence of the two PES involved on the coordinate Z. The desorption yield as a function of the residence time t_n seems to be ''converging'' with increasing dimensionality. 4D studies in which the lateral translational coordinate X is also taken into account, are presently performed. In Fig. 9 we show the desorption probability for different initial eigenstates of the electronic ground-state PES. An influence of the molecule–surface vibration on the microscopic desorption mechanism is not observed: The first four molecule–surface vibrational levels exhibit the same dependence of the asymptotic desorption probability on the residence time t_n. This is due to the weak center-of-mass distance dependence of the electronically excited-state PES at the Franck–Condon point. The minor importance of the center-of-mass distance coordinate for the microscopic desorption mechanism becomes already obvious from the small amplitude of the $\langle Z\rangle$ oscillation in Fig. 6 and the very low desorption probability found in the 1D calcula-

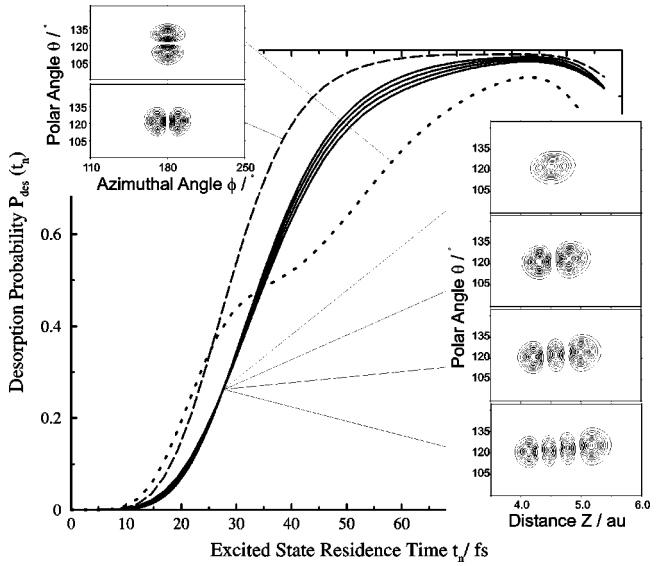

FIG. 9. Desorption probability $P_{\mathrm{des}}(t_n)$ for different initial eigenstates of the electronic ground-state PES; the four curves in the center belong to the first four molecule–surface vibrational levels, *Dashed*: Initial state with azimuthal node, *Dotted*: Initial state with node in θ.

tions shown in Fig. 8. The eigenstate with an azimuthal node (dashed curve in Fig. 9), on the other hand, leads to significantly higher desorption probabilities than the rovibrational ground state. The reason is that the increased extension of this state in the ϕ coordinate allows for a more efficient desorption since the electronic ground-state PES is repulsive as soon as the CO-molecule leaves its Cr–Cr inline configuration after laser excitation. So, desorption becomes efficient at shorter residence times of the wave packet on the PES of the $a\,^3\Pi$-like state if the selected eigenstate is "pre-excited" with respect to the azimuthal motion as compared to the lowest rovibrational eigenstate.

The same argument holds for an eigenstate which is excited in the θ coordinate (dotted curve in Fig. 9). The larger extension of this state with respect to θ as compared with the rovibrational ground state enhances the desorption probability as well. This is also caused by the topology of the electronic ground state, which becomes repulsive when the polar angle θ significantly deviates from its equilibrium value of 120°. At residence times of about 30–40 fs the node of this θ excited eigenstate accounts for a saddle-point within the $P_{\mathrm{des}}(t_n)$ function. At a propagation time of about 30–40 fs on the excited-state PES this node is located in the "critical" region for desorption. Due to the ϕ-symmetry of the potential energy surfaces this saddle-point does not occur for the ϕ-"pre-excited" eigenstate.

The considerations presented so far yield insight into the microscopic desorption mechanism. Additional insight is gained after applying lifetime averaging with respect to the resonance lifetime τ. A lifetime averaged desorption probability allows for a direct comparison with experimental results

$$P_{\mathrm{des}}(t;\tau)=\frac{\sum_{n=1}^{n_{\max}} P_{\mathrm{des}}(t,t_n)\exp\left(-\frac{t_n}{\tau}\right)}{\sum_{n=1}^{n_{\max}} \exp\left(-\frac{t_n}{\tau}\right)}. \tag{9}$$

As many as 80 single three-dimensional quantum trajectories ($n_{\max}=80$) had to be calculated for the $T=0$ K limiting case to get converged results for $P_{\mathrm{des}}(t;\tau)$. For more detailed information on the parameters of the averaging procedure see Table I. Figure 8 (bottom) shows this averaged desorption yield as a function of the external parameter τ, which is the resonance lifetime of the CO*-intermediate. The correlation between the calculated desorption yield per excitation event and the experimental desorption cross section is not straightforward. For the system $CO–Cr_2O_3$ we estimate the desorption yield to be between 1%–10%. This estimate is based on isotopic measurements for metallic adsorbate–substrate systems[47] and on the fact that in case of oxidic systems the desorption cross sections are one to four orders of magnitude larger than for metallic systems.[31] A resonance lifetime of the CO*-intermediate between 5 and 15 fs can then be estimated from our 3D studies. This lifetime is shorter than the value of 25 fs estimated for the NO^- intermediate in the photodesorption of NO from NiO(100) that was studied in two dimensions recently.[21]

E. Velocity distributions and rotational alignment

The velocity distributions of the desorbing CO-molecules shown in Fig. 10 enable further comparison with experiment. The velocity distributions, i.e., the probability distribution of the desorbed part of the wave packets in momentum space, are lifetime averaged with respect to a representative resonance lifetime of $\tau=10$ fs. This value corresponds to a desorption probability per excitation event of about 5%. Averaging with respect to the rotational state of CO has been performed as well. The different distributions in Fig. 10 result from different initial eigenstates of the electronic ground state in the excitation–de-excitation cycles. The distributions are located roughly in the experimental range between 0 and 2000 m/s.

In the experiments reported in Sec. II, the alignment of the total angular momentum vector J has been measured. The projection of J onto the surface normal is given by the quantum number M. One has to distinguish between alignment and orientation. The desorbing molecules are aligned if the population of high $|M|$-values is different from the population of low $|M|$-values. Orientation means that the populations of positive and negative M-values differ. The quadrupole moment A_0^2 is a measure of the rotational alignment and is defined as[33]

$$A_0^2(J)=\left\langle J\left|\frac{3M^2-J^2}{J^2}\right|J\right\rangle. \tag{10}$$

The quadrupole moment can be numerically lifetime averaged according to

$$A_0^2(J,\tau)=\frac{\sum_{n=1}^{n_{\max}} \exp\left(-\frac{t_n}{\tau}\right)\Sigma_M\left(\frac{3M^2-J^2}{J^2}\right)P_J(M,t_n)}{\sum_{n=1}^{n_{\max}} \exp\left(-\frac{t_n}{\tau}\right)P_J(M,t_n)}, \tag{11}$$

with

$$P_J(M,t_n)=\int_0^{\infty}\Psi^*_{\mathrm{des}}(k_z,J,M)\Psi_{\mathrm{des}}(k_z,J,M)\,dk_z. \tag{12}$$

In the evaluation of Eq. (11) the desorbed part of the wave function, separated by the grid change technique presented in Sec. IV A, was used. Figure 11 shows the calculated quadrupole moment A_0^2 as a function of the rotational quantum number J together with the experimental observations. The values have been averaged with respect to the CO desorption velocity. Again, a representative excited-state resonance lifetime of $\tau=10$ fs has been chosen, corresponding to a desorption probability per excitation event of about 5%. In Fig. 11 several cases are studied:

If one starts from the rovibrational ground-state eigenfunction ($T=0$ K case), helicopter motion is found at medium rotational excitation which changes to cartwheel motion with increasing J. This is in qualitative agreement with the experimental observation. However, at low rotational quanta J our simulations differ from the experimental values in the $T=0$ K limit.

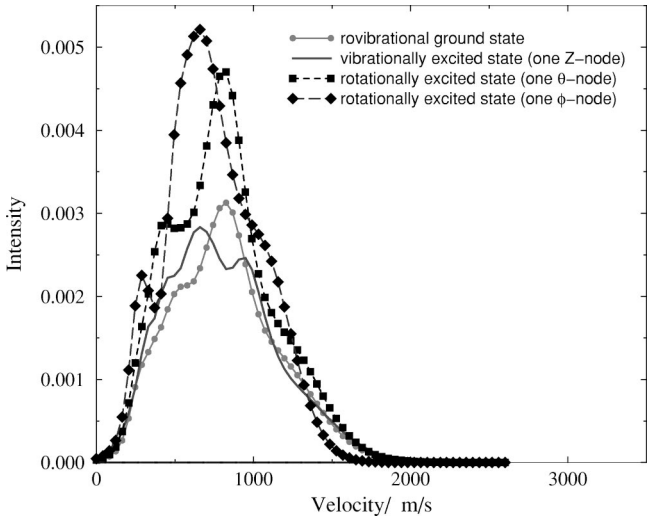

FIG. 10. Asymptotic velocity distributions for an averaged resonance lifetime $\tau = 10$ fs for different eigenstates of the electronic ground-state PES. The velocity distributions are averaged with respect to the rotational state of the desorbing CO-molecule.

The agreement at low J is better if the frustrated rotational level with one node in ϕ is pre-excited. The microscopic reason is that this level has larger helicopter character from the very beginning of the DIET simulation. This feature survives within the excitation–de-excitation cycle and the following lifetime averaging. It yields high helicopter character of the desorbing CO throughout the entire J-range, disagreeing with the experimental values at large J. Due to the relative populations of the nuclear eigenstates given in Sec. IV B a temperature averaged result will look very much like the $T = 0$ K result. The molecule–surface vibrational levels do not yield significant different curves for the quadrupole moment as a function of J and are not shown in Fig. 11. This behavior again emphasizes the minor role of the desorption coordinate Z for the microscopic desorption mechanism in this system.

To understand why helicopter motion is observed in general, we have switched the azimuthal gradients of the potential energy surfaces on and off. After switching the ϕ-gradient off we have the situation of flat uncorrugated surfaces.

As can be seen in Fig. 11, a combination of two flat uncorrugated states within the DIET-cycle yields cartwheeling CO-molecules in the entire J-range. In this case there is no driving force for helicopter motion in the entire system.

We do not get any helicopter motion as well, if only the excited state ϕ-gradient is switched off. From a mechanistic point of view this is reasonable, since the CO-molecule does not get its helicopter kick after laser excitation any more. Apart from spreading, the molecule rests in its ground-state equilibrium position with respect to ϕ during the entire simulation. Acceleration can only occur with respect to the polar angle θ, therefore, only cartwheel motion is found.

However, the helicopter kick in the excited state is also not sufficient to explain the helicopter motion of the desorbing molecule. Turning off the ground-state ϕ-gradient and keeping the excited-state ϕ-corrugation one gets also only cartwheeling CO-molecules in the entire J-range.

It is the combination of the ϕ-gradient in the excited state *and* the ground-state ϕ-corrugation which induces the helicopter motion of the desorbing molecule. The mechanistic picture is such that after laser excitation the CO molecule is forced out of its ground-state geometry with respect to ϕ. After being transferred back to the electronic ground state, the CO molecule experiences an opposite ϕ-gradient which accelerates the molecule backwards towards its equilibrium geometry. This excitation–de-excitation cycle excites helicopter motion. Evidence for this process can be found in the 1D-cuts through the PES on the left of Fig. 4.

The present mechanistic picture has been obtained by taking into account our two representative *ab initio* PES. Especially their angular topologies could not have been guessed on an empirical basis. Nevertheless we have to keep in mind that there is considerable disagreement at low J-values. There are four possible reasons for this deviation:

(1) For small J experimental uncertainties exist,[29] since the quadrupole moment has been derived from experimental spectra within the classical vector approximation which is only valid in the large J limit.[29,33]
(2) For very small J, our picture of a helicopter molecule is not meaningful. The perfect helicopter molecule has its angular momentum vector J directed perpendicular to the molecular axis. In the very low J regime, this case cannot occur, because the projection of J onto the surface normal does not approach the length of the J vector itself.
(3) Of course, also the question of the accuracy of our *ab initio* calculations arises. As shown in Fig. 11, the quadrupole moment is strongly influenced by the azimuthal dependence of the potential energy surfaces. We showed that helicopter motion is a result of a delicate interplay of azimuthal forces. However, since our ground-state calculation underestimates the adsorption energy by about 0.2 eV,[28] we expect an overestimation of the equilibrium distance of the molecule from the surface. Thus, the azimuthal surface corrugation in the electronic ground state could be too small in our *ab initio* calculations. A larger azimuthal gradient within the electronic ground state would promote helicopter motion.
(4) Finally, our discussion is limited by the restriction of our model to three dimensions and by the possibility of a CO^--intermediate to be involved in the photodesorption process.

The choice of the resonance lifetime of the excited state as the only external parameter did not influence the calculated quadrupole moment and the velocity distributions significantly as long as the value of τ remained between 5 and 15 fs.

V. CONCLUSIONS

In this study the photodesorption of the CO–Cr_2O_3(0001) system was treated systematically on a complete *ab initio* basis. The time-dependent Schrödinger equation was solved in three dimensions (the desorption co-

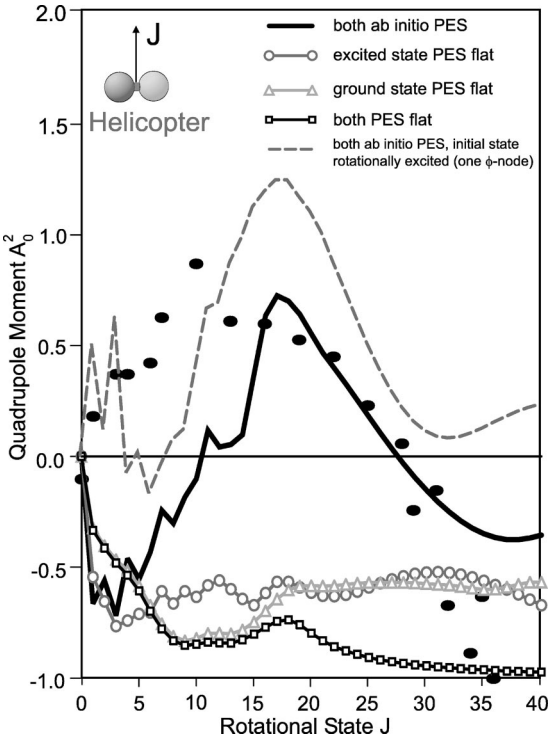

FIG. 11. Quadrupole moment for the desorption of CO from Cr_2O_3 as a function of rotational excitation, averaged with respect to the desorption velocity; the resonance-lifetime of the CO*-intermediate has been chosen as $\tau = 10$ fs in coincidence with a reasonable desorption probabilty. Filled circles: Experimental data points.

ordinate and two angular coordinates) for a two-state model. The two electronic states involved are the electronic ground state of the adsorbate–substrate system and an electronically excited state generated by an internal CO ($5\sigma \rightarrow 2\pi^*$) excitation at a laser irradiation of 6.4 eV. The PES of both states were calculated by quantum chemical *ab initio* methods.

There are several conclusions from the quantum dynamical calculations as far as the microscopic desorption mechanism is concerned: A one-dimensional treatment in the desorption coordinate Z, as performed very often in former studies, is not sufficient for this system. The desorption is strongly coupled to the polar angle θ. The inclusion of this coordinate enlarges the desorption efficiency drastically. The mechanistic reason for this increase in desorption efficiency is that the CO-molecule moves from the strongly tilted adsorption geometry in the electronic ground state towards an upright adsorption geometry after laser excitation. After relaxation back to the electronic ground state the CO molecule feels a repulsive potential. The resonance lifetime of the CO*-intermediate is between 5 and 15 fs. This is a shorter lifetime than in case of the oxide system NO–NiO(100) studied recently.[21]

The azimuthal corrugations of both the electronically excited and the ground-state PES are responsible for the helicopter motion of the desorbing molecule. Helicopter motion is excited in two steps: First the CO-molecule is kicked out of its inline adsorption geometry after laser irradiation by the ϕ-gradient in the excited state. The ϕ-gradient in the excited state is not large enough though to account for a helicopter motion of rotationally hot molecules. After relaxation to the electronic ground state the CO-molecule experiences the ϕ-corrugation of the ground state which drives it in the opposite direction towards the inline configuration.

However, at low rotational quanta our three-dimensional model quantitatively disagrees with the experimental features. Nevertheless, we clearly gain microscopic insight into the desorption mechanism and a qualitative agreement with the experimental quadrupole moment. The discrepancies between experiment and theory have to be addressed by further experimental and theoretical investigations.

With an excited-state resonance lifetime of 10 fs the velocity distribution of the desorbing species is located in the experimental range. At the experimental temperature of $T = 100$ K only molecule–surface vibrational levels are significantly populated. These have no significant influence on the desorption efficiency and the rotational alignment of the desorbing CO. On the other hand, the ''frustrated'' rotational levels do influence those observables. Especially, the state with a node in the azimuthal angle ϕ enlarges the desorption efficiency and accounts for an increased helicopter character of the desorbing CO-molecule. This illuminates the importance of the angular coordinates for the microscopic picture of the desorption mechanism. For the mechanistic understanding of the desorption experiments at $T = 100$ K it is sufficient though to consider the rovibrational ground state of the electronic ground state PES.

For future investigations it is challenging to further increase the dimensionality of the quantum dynamical calculations. Four-dimensional *ab initio* PES for both states involved, in which also the frustrated translation X is included, are already available.[28,41] Four-dimensional time-dependent wave packet calculations on *ab initio* PES for the ground and excited state will provide a benchmark study. More approximate schemes (in the dynamic as well as the electronic structure part) could very well be calibrated to our study. A future goal is the parameter-free simulation of a DIET-process in as many dimensions as possible. It is also challenging to combine the presented high-dimensional calculations with methological improvements. In this sense dissipative quantum dynamics in combination with the explicit treatment of the experimental laser pulse as an external perturbation is currently studied. Finally, the possibility of a CO^- resonance as a short-lived intermediate has to be eludicated.

ACKNOWLEDGMENTS

We gratefully acknowledge financial support by the German Israeli Foundation (GIF) and by the German Science Foundation (DFG, SPP1093). We thank Dr. D. Lemoine for many valuable discussions.

[1] M. Bonn, S. Funk, C. Hess, D. N. Denzler, C. Stampfl, M. Scheffler, M. Wolf, and G. Ertl, Science **285**, 1042 (1999).
[2] V. May and O. Kühn, *Charge and Energy Transfer Dynamics in Molecular Systems* (Wiley VCH, New York, 2000).
[3] D. Menzel and R. Gomer, J. Chem. Phys. **41**, 3311 (1964).
[4] P. A. Redhead, Can. J. Chem. **42**, 886 (1964).
[5] P. R. Antoniewicz, Phys. Rev. B **21**, 3811 (1980).
[6] H. Guo, P. Saalfrank, and T. Seideman, Prog. Surf. Sci. **62**, 239 (1999).
[7] H. Guo, J. Chem. Phys. **106**, 1967 (1997).

[8] P. Saalfrank, G. Boendgen, K. Finger, and L. Pesce, Chem. Phys. **251**, 51 (2000).
[9] N. Chakrabarti, V. Balasubramanian, N. Sathyarmurthy, and J. Gadzuk, Chem. Phys. Lett. **242**, 490 (1995).
[10] F. M. Zimmermann, Surf. Sci. **390**, 174 (1997).
[11] L. Pesce, T. Gerdts, U. Manthe, and P. Saalfrank, Chem. Phys. Lett. **288**, 383 (1998).
[12] A. R. Burns, E. B. Stechel, D. R. Jennison, and Y. S. Li, J. Chem. Phys. **101**, 6318 (1994).
[13] T. Hertel, M. Wolf, and G. Ertl, J. Chem. Phys. **102**, 3414 (1995).
[14] H. Guo and T. Seideman, J. Chem. Phys. **103**, 9062 (1995).
[15] P. Saalfrank, Surf. Sci. **390**, 1 (1997).
[16] P. Saalfrank, Chem. Phys. **211**, 265 (1996).
[17] R. Baer and R. Kosloff, J. Chem. Phys. **106**, 8862 (1997).
[18] R. Baer, Y. Zeiri, and R. Kosloff, Phys. Rev. B **55**, 10952 (1997).
[19] C. Meier and D. Tannor, J. Chem. Phys. **111**, 3365 (1999).
[20] T. Klamroth and P. Saalfrank, J. Chem. Phys. **112**, 10571 (2000).
[21] T. Klüner, H.-J. Freund, V. Staemmler, and R. Kosloff, Phys. Rev. Lett. **80**, 5208 (1998).
[22] T. Klüner, S. Thiel, H.-J. Freund, and V. Staemmler, Chem. Phys. Lett. **294**, 413 (1998).
[23] A. Gross, S. Wilke, and M. Scheffler, Phys. Rev. Lett. **75**, 2718 (1995).
[24] I. Beauport, K. Al-Shamery, and H.-J. Freund, Chem. Phys. Lett. **256**, 641 (1996).
[25] S. Thiel, M. Pykavy, T. Klüner, H.-J. Freund, R. Kosloff, and V. Staemmler, Phys. Rev. Lett. **87**, 077601 (2001).
[26] F. Rohr, M. Bäumer, H.-J. Freund, J. A. Mejias, V. Staemmler, S. Müller, L. Hammer, and K. Heinz, Surf. Sci. **372**, L 291 (1997).
[27] F. Rohr, M. Bäumer, H.-J. Freund, J. A. Mejias, V. Staemmler, S. Müller, L. Hammer, and K. Heinz, Surf. Sci. **389**, 391 (1997).
[28] M. Pykavy, V. Staemmler, O. Seiferth, and H.-J. Freund, Surf. Sci. **479**, 11 (2001).
[29] D. C. Jacobs and R. N. Zare, J. Chem. Phys. **85**, 5457 (1986).
[30] T. Mull, B. Baumeister, M. Menges, H.-J. Freund, D. Weide, C. Fischer, and P. Andresen, J. Chem. Phys. **96**, 7108 (1992).
[31] M. Menges, B. Baumeister, K. Al-Shamery, H.-J. Freund, C. Fischer, and P. Andresen, J. Chem. Phys. **101**, 3318 (1994).
[32] G. Eichhorn, M. Richter, K. Al-Shamery, and H. Zacharias, J. Chem. Phys. **111**, 386 (1999).
[33] C. Greene and R. N. Zare, J. Chem. Phys. **78**, 6741 (1983).
[34] V. Staemmler, Theor. Chim. Acta **45**, 89 (1977).
[35] J. Wasilewski, Int. J. Quantum Chem. **36**, 503 (1989).
[36] U. Meier and V. Staemmler, Theor. Chim. Acta **76**, 95 (1989).
[37] R. Fink and V. Staemmler, Theor. Chim. Acta **87**, 129 (1993).
[38] S. F. Boys and F. Bernardi, Mol. Phys. **19**, 553 (1970).
[39] C. Xu, B. Dillmann, H. Kuhlenbeck, and H.-J. Freund, Phys. Rev. Lett. **67**, 3551 (1991).
[40] F. Zimmermann and W. Ho, Surf. Sci. Rep. **22**, 127 (1995).
[41] M. Pykavy, S. Thiel, T. Klüner, H.-J. Freund, and V. Staemmler (unpublished).
[42] R. Kosloff, in *Numerical Grid Methods and Their Application to Schrödinger's Equation*, edited by C. Cerjan (NATO ASI Series, Kluwer Academic, Dordrecht, 1992).
[43] R. Heather and H. Metiu, J. Chem. Phys. **86**, 5009 (1987).
[44] G. C. Corey and D. Lemoine, J. Chem. Phys. **97**, 4115 (1992).
[45] M. D. Feit, J. Fleck, Jr., and A. Steiger, J. Comput. Phys. **47**, 412 (1982).
[46] R. Kosloff, J. Phys. Chem. **92**, 2087 (1988).
[47] J. W. Gadzuk, L. R. Richter, S. A. Buntin, D. S. King, and R. R. Cavanagh, Surf. Sci. **235**, 317 (1990).
[48] J. W. Gadzuk, Surf. Sci. **342**, 345 (1995).
[49] R. Kosloff and H. Tal-Ezer, Chem. Phys. Lett. **127**, 223 (1986).
[50] *Femtosecond Chemistry*, edited by J. Manz and L. Wöste (VCH Weinheim, New York, Cambridge, Tokyo, 1995).